Biophysical and mutagenic analysis of *Thermoanaerobacter ethanolicus* secondary-alcohol dehydrogenase activity and specificity

Douglas S. BURDETTE*, Francesco SECUNDO†, Robert S. PHILLIPS‡§, Jun DONG‡, Robert A. SCOTT‡§ and J. Gregory ZEIKUS*‖[1]

*Department of Biochemistry, Michigan State University, East Lansing, MI 48824-1319, U.S.A., †Instituto di Chimica degli Ormoni, CNR, Milan, Italy, ‡Center for Metalloenzyme Studies, University of Georgia, Athens, GA 30601-2556, U.S.A., §Department of Chemistry, University of Georgia, Athens, GA 30602-2556, U.S.A., and ‖Michigan Biotechnology Institute, Lansing, MI 48909, U.S.A.

The *Thermoanaerobacter ethanolicus* 39E *adhB* gene encoding the secondary-alcohol dehydrogenase (2° ADH) was overexpressed in *Escherichia coli* at more than 10% of total protein. The recombinant enzyme was purified in high yield (67%) by heat-treatment at 85 °C and $(NH_4)_2SO_4$ precipitation. Site-directed mutants (C37S, H59N, D150N, D150E and D150C were analysed to test the peptide sequence comparison-based predictions of amino acids responsible for putative catalytic Zn binding. X-ray absorption spectroscopy confirmed the presence of a protein-bound Zn atom with $ZnS_1(imid)_1(N,O)_3$ co-ordination sphere. Inductively coupled plasma atomic emission spectrometry measured 0.48 Zn atoms per wild-type 2° ADH subunit. The C37S, H59N and D150N mutant enzymes bound only 0.11, 0.13 and 0.33 Zn per subunit respectively, suggesting that these residues are involved in Zn liganding. The D150E and D150C mutants retained 0.47 and 1.2 Zn atoms per subunit, indicating that an anionic side-chain moiety at this position preserves the bound Zn. All five mutant enzymes had $\leqslant 3\%$ of wild-type catalytic activity, suggesting that the *T. ethanolicus* 2° ADH requires a properly co-ordinated catalytic Zn atom. The His-59 and Asp-150 mutations also altered 2° ADH affinity for propan-2-ol over a 140-fold range, whereas the overall change in affinity for ethanol spanned a range of only 7-fold, supporting the importance of the metal in 2° ADH substrate binding. The lack of significant changes in cofactor affinity as a result of these catalytic Zn ligand mutations suggested that 2° ADH substrate- and cofactor-binding sites are structurally distinct. Altering Gly^{198} to Asp reduced the enzyme specific activity 2.7-fold, increased the K_m(app) for $NADP^+$ 225-fold, and decreased the K_m(app) for NAD^+ 3-fold, supporting the prediction that the enzyme binds nicotinamide cofactor in a Rossmann fold. Our data indicate therefore that, unlike the liver 1° ADH, the Rossmann-fold-containing *T. ethanolicus* 2° ADH binds its catalytic Zn atom using a sorbitol dehydrogenase-like Cys-His-Asp motif and does not bind a structural Zn atom.

INTRODUCTION

Alcohol dehydrogenases (ADHs), central to prokaryotic and eukaryotic metabolism, are also potential biocatalysts for chiral chemical production [1–6]. The functionally and presumably structurally similar ADHs are classified as primary or secondary based on their higher catalytic efficiencies toward primary (1°) or secondary (2°) alcohols. These typically homodimeric or homotetrameric enzymes are almost exclusively Zn-containing metalloenzymes [7] that use NAD(H) (EC 1.1.1.1), NADP(H) (EC 1.1.1.2) or both (EC 1.1.1.71) as cofactor. Fe-linked [8] and ferredoxin F_{240}-dependent [9] 1° ADHs have also been reported. The catalytic role of Zn in liver 1° ADH activity has been proposed to involve binding directly to the substrate oxygen atom, facilitating hydride transfer between the adjacent substrate carbon atom and the nicotinamide cofactor [7,10–12]. Although 1° ADHs from diverse sources have been extensively characterized [7], little is known about the molecular basis for their substrate specificity. Far less is known about 2° ADH structure–function, with relatively few reported studies on enzyme purification and characterization [13–17] and a complete lack of site-directed mutagenic information. Recent reports of thermophilic and mesophilic 2° ADH crystallization and X-ray diffraction [18–20] provide the promise of exact structural data; however, the inability of structural characterization alone to explain 1° ADH catalytic properties underscores the importance of a multidisciplinary approach to 2° ADH structure–function research. Because of the central metabolic roles of 2° ADHs [17,21] and their potential biotechnological value [1–6,22,23], structure–function analysis of catalysis and substrate specificity would contribute significantly to the basic understanding of enzyme function and to biocatalyst design.

The exact three-dimensional structure of horse liver 1° ADH has been determined [24], indicating that the catalytic Zn atom is bound by two Cys and one His residue and that the nicotinamide cofactor is bound in a Rossmann fold [7,25]. Research to date has failed to identify the ADH active-site residues specifically responsible for substrate binding. The presumed similarity, based on shared catalytic properties, between 1° and 2° ADH structures provided the rationale for sequence-based comparisons between these enzymes [26–28]. Peptide sequence alignments of thermophilic and mesophilic 1° and 2° ADHs were used to hypothesize (i) that 2° ADHs bind their nicotinamide cofactor in a Rossmann fold, (ii) that they lack a structural Zn-binding loop, and (iii) that they use a unique Cys-His-Asp (Cys^{37}-His^{59}-Asp^{150}) motif for catalytic metal liganding [28]. Chemical-modification experiments have implicated Zn, Cys and His in *Thermoanaerobium brockii* and *Thermoanaerobacter ethanolicus* 39E 2° ADH ca-

Abbreviations used: ADH, alcohol dehydrogenase; XAS, X-ray absorption spectroscopy; ICP-AES, inductively coupled plasma-atomic emission spectrometry.

[1] To whom correspondence should be addressed.

talysis [13,28], but validation of the predicted Zn-liganding motif awaited assessment by biophysical characterization and site-directed mutagenesis. The strong similarities among 2° ADH peptide sequences, kinetic parameters, subunit compositions and molecular masses [28,29] suggest that the results of the *T. ethanolicus* 2° ADH structure–function analysis will be generally applicable to other 2° ADHs.

The research reported here involves the development of a recombinant overexpression and purification system providing high yields of homogeneous enzyme. The roles of *T. ethanolicus* 2° ADH amino acids Cys^{37}, His^{59} and Asp^{150} as catalytic Zn-binding ligands and of Gly^{198} as the single residue responsible for NADP(H) specificity are assessed from site-directed mutation effects on enzyme K_m(app), V_{max}(app), Zn and cofactor binding. X-ray absorption spectroscopic (XAS) studies support this catalytic Zn-co-ordination sphere. Finally, kinetic data on 2° ADH mutants and exact structural information on 1° ADHs are used to create a hypothetical working model for the 2° ADH active site and to distinguish key differences between 2° and 1° ADH structure–function relationships.

MATERIALS AND METHODS

Chemicals and reagents

All chemicals were reagent/molecular biology grade or purer. Oligonucleotide synthesis and amino acid sequence analysis were performed by the Macromolecular Structure Facility, Department of Biochemistry, Michigan State University. The kanamycin-resistance GenBlock (*Eco*RI) DNA cartridge used in expression vector construction was purchased from Pharmacia (Uppsala, Sweden) [30]. DNA for sequencing was isolated using the Wizard Miniprep kit (Promega, Madison, WI, U.S.A.).

Media and strains

Escherichia coli (DH5α) containing the 2° ADH recombinant plasmids were grown in rich complex medium (20 g/l tryptone, 10 g/l yeast extract, 5 g/l NaCl) at 37 °C in the presence of 25 μg/ml kanamycin and 100 μg/ml ampicillin.

Mutagenesis

All DNA manipulations were performed using established protocols [31,32]. Point mutations were introduced into the *T. ethanolicus* 39E *adhB* gene by PCR [31] using plasmid pADHB25-kan [28] as template. An oligonucleotide primer (KA4N) was synthesized complementary to the non-coding strand that included a *KpnI* restriction site, the native *adhB* ribosome assembly site, and the *adhB* translation initiation codon (5′-CGG***GGTACC***CCGTATTTTAGGAGGTGTTTAATGATGAAAGG-3′). A second oligonucleotide primer (KA4C) that included the complement to the *adhB* termination codon and an *ApaI* restriction site (5′-CAGTCC***GGGCCC***TTATGCTAATATTACAACAGGTTTG-3′) was synthesized complementary to the coding strand. Oligonucleotide 1M1N was identical with primer KA4N except for the substitution of TTA for ATG at positions 31–33. Complementary 30–45-base oligonucleotide primers that contained the mutated bases (C37S: coding, 5′-GCTGTGGCCCCTT**C**CACTTCGGACATTCATACC-3′, non-coding, 5′-GGTATGAATGTCCGAAGT**G**GAAGGGGC-3′; H59N: coding, 5′-CATGATACTCGGT**A**ACGAAGCTGTA-3′, non-coding, 5′-CTTCACCTACAGCTTCGT**T**ACCGAG-3′; D150N: coding, 5′-GGAAGCTGCACTTATGATTCCC**A**ATATGATGACCACTGG-3′; non-coding, 5′-GCTCCGTGAAAACCAGTGGTCATCATAT**T**GGGAATCATA-3′; D150C: coding, 5′-GGAAGCTGCACTTATGATTCCC**TG**TATGATGACCACTGG-3′, non-coding, 5′-GCTCCGTGAAAACCAGTGGTCATCA-TA**CA**GGGAATCATAAG-3′; D150E: coding, 5′-GGAAGCTGCACTTATGATTCCCGA**A**ATGATGACCACTGG-3′, non-coding, 5′-GCTCCGTGAAAACCAGTGGTCATCAT**T**TCGGGAATCATA-3′; G198D: coding, 5′-GAATTATTGCCGTAG**A**CAGTAGACCAGTTTGTG-3′, non-coding, 5′-CACAAACTGGTCTACTGTC**T**ACGGCAATAATTC-3′) were used in conjunction with the two KA4 end primers to amplify the N-terminal and C-terminal segments of the *adhB* gene. PCR syntheses of partial and complete mutated genes were performed using the Taqplus exonuclease-containing polymerase reagent (Strategene, LA Jolla, CA, U.S.A.). All clones were expressed in pBluescriptII KS(+) containing a kanamycin-resistance cartridge introduced into the polylinker *Eco*RI site. Mutations were verified by DNA sequencing using the method of Sanger et al. [33].

Enzyme purification

The recombinant enzyme was purified from *Escherichia coli* (DH5α) aerobically. The pelleted cells from batch cultures were resuspended (0.5 g wet wt./ml) in buffer A (50 mM Tris/HCl, pH 8.0, 5 mM dithiothreitol and 10 μM $ZnCl_2$) containing 3 μg/ml lysozyme. The resuspended cells were incubated on ice for 30 min, frozen in liquid N_2, thawed, and centrifuged for 30 min at 15000 ***g***. The clarified lysate was incubated at 85 °C for 15 min, cooled on ice for 30 min, and then centrifuged for 30 min at 15000 ***g***. $(NH_4)_2SO_4$ (50 %, w/v) was added to the supernatant and stirred at 4 °C for 30 min. The 2° ADH was recovered from the supernatant after centrifugation for 30 min at 15000 ***g*** and precipitated with stirring at 4 °C for 30 min in 70 % (w/v) $(NH_4)_2SO_4$. After centrifugation for 30 min at 15000 ***g***, the purified 2° ADH was resuspended in buffer A and stored at 4 °C.

Enzyme kinetics

The standard 2° ADH activity assay was defined as $NADP^+$ reduction coupled to propan-2-ol oxidation at 60 °C as previously described [17]. The enzyme was incubated at 55 °C for 15 min before activity determination. Tris buffer pH was adjusted at 25 °C to be 8.0 at 60 °C (thermal correction factor = −0.031 ΔpH/°C). Assays to determine K_m(app) and V_{max}(app) were conducted at 60 °C with substrate concentrations between $20 \times K_m$(app) and $0.2 \times K_m$(app). Kinetic parameters were calculated from non-linear best fits of the data to the Michaelis–Menten equation using Kinzyme software [34] on an IBM personal computer. Protein concentrations were measured using the bicinchoninic acid procedure (Pierce, Rockford, IL, U.S.A.). Kinetic parameter values were calculated from the mean ± S.D. for at least three independent activity determinations.

Determination of Zn content, molecular mass and peptide sequence

2° ADH samples were dialysed against 50 mM NH_4HCO_3, pH 8.0, containing 100 g/l Chelex resin (Bio-Rad, Hercules, CA, U.S.A.) for 12 h to remove unbound or adventitiously bound metals. The metal-cleared samples were concentrated to between 1.2 and 12 mg/ml using Centricon 30 ultrafiltration units (Amicon, Beverly, MA, U.S.A.) for inductively coupled plasma-atomic emission spectrometry (ICP-AES) analysis (Chemical Analysis Laboratory at the University of Georgia, Athens). Subunit molecular-mass values were determined by comparison with standards (Bio-Rad) using SDS/PAGE (12 % polyacrylamide). The error values for the N-terminal amino acid sequences

of the recombinant 2° ADH protein population expressed from the pADHBKA4-kan plasmid were reported as standard deviations and were calculated on the basis of the relative abundances of the two amino acid species present at each of the first seven peptide positions.

XAS

The Zn-co-ordination environment was structurally characterized using EXAFS. Enzyme samples were concentrated to 1–10 mg/ml (~ 0.1 mM Zn) in 50 mM Tris/HCl, pH 8.0 and stored in liquid N_2 before analysis. Zn EXAFS data were collected at the Stanford Synchrotron Radiation Laboratory (beamline 7–3) with the SPEAR ring operating at 3.0 GeV and 55–65 mA. Details of data collection and reduction were as follows: monochrometer crystal [Si(220)]; fluorescence detection using a 13-element solid-state array; data are the average of 16 scans (22 min); temperature, 10 K; energy calibration, 9660.7 eV for the first inflection of the Zn foil spectrum; E_0, 9670 eV; pre-edge background energy range, 9333–9625 eV; pre-edge background Gaussian centre (width = 1000 eV), 8713 eV; spline background was a third-order polynomial from 9675 to 10366 eV with spline points at 9905 and 10136 eV.

EXAFS data were analysed by established techniques [35] using EXAFSPAK software (courtesy of G. N. George, Stanford, CA). Raw EXAFS data curve fitting to identify and quantify co-ordination by histidine imidazoles included single and multiple scattering paths 4.5 Å or less from the Zn atom. The geometry and orientation for an imidazole bond to Zn were fixed on the basis of those for the model compound $Zn(imid)_4(NO_3)_2$ [36]. Theoretical scattering amplitudes and phase shifts for each scattering path containing four or fewer legs were calculated using FEFF v5.04 software [37–39]. These calculated parameters were used in a constrained curve-fitting process in which the numbers of Zn-co-ordinating atoms were limited to integer values. In fits with imidazoles as the only (N,O)-containing ligands, the distances and Debye–Waller factors for outer-shell imidazole rings were constrained to a given ratio with the first-shell (Zn–N) distance and Debye–Waller factor respectively. Similar FEFF-based analysis of data also collected at 10 K for model compounds containing M–imidazole (M = Ni, Cu, Zn) interactions yielded imidazole first- ($R' \approx 2$ Å), second- ($R' \approx 3$ Å) and third ($R' \approx 4$ Å) shell σ_{as}^2 values of 0.0020–0.0030 Å^2, 0.0030–0.0050 Å^2 and 0.0040–0.0060 Å^2 respectively. Numerous fits using other first-shell (N,O)-containing ligands at distances indistinguishable from that for $Zn–N_{imid}$ were examined. In these fits, the Debye–Waller factor for the Zn–(N,O) first-shell was not constrained to be a particular ratio with the second- and third-shell values since static disorder in such a mixed-ligand shell is expected to result in larger relative Debye–Waller σ_{as}^2 values. Calibration with $Zn(imid)_4(NO_3)_2$ and Zn–S ($[Zn(S_4)_2]^{2-}$) model compounds [40] indicated accuracies within 0.02 Å for the first-shell distances reported here.

RESULTS

Enzyme overexpression

T. ethanolicus 2° ADH was purified from *E. coli* (DH5α) harbouring plasmid pADHBKA4-kan (Table 1) with a 67% recovery. The recombinant enzyme was expressed at more than 10% of total soluble protein without induction (Figure 1). This construct contained the native ribosome assembly site and translational initiation codons but lacked the native promoter regions, placing the gene under transcriptional control of the pBluescriptII KS(+) lacZ promoter. The recombinant protein

Table 1 Purification of the recombinant wild-type 2° ADH expressed from plasmid pADHBKA4-kan

A unit of activity is defined as the reduction of 1 μmol of $NADP^+$/min during propan-2-ol oxidation under standard assay conditions.

Purification step	Total protein (mg)	Total activity (units)	Protein concentration (mg/ml)	Specific activity (units/mg)	Purification (fold)	Yield (%)
Cell extract	59	270	8.7	4.8		100
Heat-treatment	25	280	4.6	11	2.3	100
$(NH_4)_2SO_4$ precipitation	4.2	180	3.4	44	9.2	67

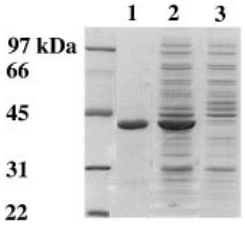

Figure 1 SDS/PAGE of wild-type recombinant 2° ADH

Lanes: 3, cell extract of *E. coli* DH5α harbouring plasmid pBluescriptIIKS(+); 2, clone KA4 cell extract; 1, clone KA4 dialysed $(NH_4)_2SO_4$ precipitate. The molecular masses of the standards flanking the sample lanes are indicated on the left. Proteins were stained with Coomassie Brilliant Blue R-250.

population included 56±11% enzyme with a duplicated N-terminal methionine (MMKGFA…) while 44±11% of the protein possessed a single methionine at the N-terminus. Alteration of the ATGATG translational initiation site to TTAATG in the pADHB1M1-kan expression plasmid eliminated the synthesis of 2° ADH with two N-terminal methionines but altered neither the enzyme expression level compared with that seen with pADHBKA4-kan nor the enzyme specific activities toward ethanol and propan-2-ol. The K_m(app) values toward propan-2-ol, ethanol and $NADP^+$ were 1.1±0.22 mM, 53±9.0 mM and 17±2.6 μM respectively for the enzyme expressed from pADHBKA4-kan and 0.87±0.32 mM, 37±4.2 mM and 8.5±1.4 μM respectively for the enzyme expressed from pADHB1M1-kan.

Catalytic Zn ligation

Chemical-modification experiments have implicated Zn, Cys and His in *T. ethanolicus* 2° ADH activity. Peptide alignments identified Cys^{37}, His^{59} and Asp^{150} as potential catalytic Zn ligands [28]. Zn XAS data of native 2° ADH (not shown) were identical with those for the recombinant wild-type 2° ADH (Figure 2). Extraction of the raw XAS data for the recombinant wild-type enzyme by Fourier filtering of the first-shell FT peak, followed by single-shell curve-fitting, suggested a $Zn(N,O)_{3–4}S_1$ first co-ordination sphere (results not shown). Non-linear least-square fits to unfiltered smoothed EXAFS data (Figure 2b) allow estimation of the number of histidine imidazole ligands. Table 2 summarizes the results obtained assuming either one or two imidazole ligands. The negative Debye–Waller σ_{as}^2 value for the Zn–S ligand and the unreasonably large $Zn–C_4$ and $Zn–N_3$ σ_{as}^2 values indicate that the co-ordination sphere $\{Zn(imid)_2(N,O)_1S_1\}$

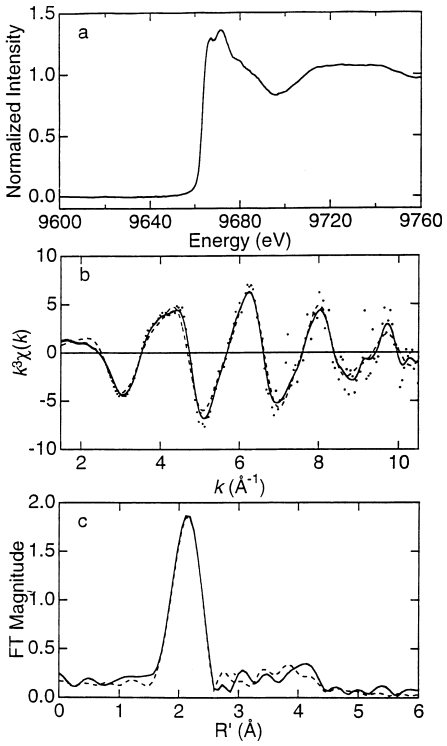

Figure 2 Zn K-edge XAS data for recombinant wild-type *T. ethanolicus* 2° ADH

(**a**) Raw XAS data in the Zn K-edge region. (**b**) plot of Fourier-transformed (FT) data versus distance for raw (····) and smoothed (——) Zn EXAFS data compared with simulation (– – – –) using parameters from fit no. 3 in Table 4. (**c**) FT of smoothed EXAFS (——) compared with FT of the simulation (– – – –). Both FTs used k^3-weighted EXAFS data over the range $k = 1.5$–10.5 Å.

Table 2 Curve-fitting results for Zn K-edge smoothed EXAFS of wild-type 2° ADH

A group is the chemical unit defined for the multiple scattering calculation (when necessary). N_s is the number of scatterers (or groups) per metal. R_{as} is the metal–scatterer distance. σ_{as}^2 is a mean square deviation in R_{as}. ΔE_0 is the shift in E_0 for the theoretical scattering functions. The f' value is calculated from a normalized error (χ^2):

$$f' = \frac{\{\Sigma_i[k^3(\chi_i^{obs} - \chi_i^{calc})]^2/N\}^{1/2}}{[(k^3\chi^{obs})_{max} - (k^3\chi^{obs})_{min}]}$$

The N_s numbers in parentheses were not varied during the optimization. Underlined values are chemically or physically unreasonable. Numbers in square brackets were constrained to be a multiple of the value immediately above.

Sample k range	Fit	Group	Shell	N_s	R_{as}(Å)	σ_{as}^2 (Å^2)	ΔE_0 (eV)	f'
Recomb. 2° ADH	1	Cys	Zn–S	(1)	2.25	−0.0012	−0.6	0.048
k = 1.5–10.5/Å		Imid + N/O	Zn–N/O	(3)	1.97	0.0012	2.3	
		Imidazole	Zn–C_5	(2)	2.92	0.0078	[2.3]	
		Imidazole	Zn–C_2	(2)	3.01	[0.0081]	[2.3]	
		Imidazole	Zn–C_4	(2)	4.06	[0.0109]	[2.3]	
		Imidazole	Zn–N_3	(2)	4.12	[0.0110]	[2.3]	
	2	Cys	Zn–S	(1)	2.26	0.0004	3.3	0.042
		Imid + N/O	Zn–N/O	(4)	1.98	0.0043	2.5	
		Imidazole	Zn–C_5	(2)	2.94	0.0081	[2.5]	
		Imidazole	Zn–C_2	(2)	3.03	[0.0083]	[2.5]	
		Imidazole	Zn–C_4	(2)	4.09	[0.0112]	[2.5]	
		Imidazole	Zn–N_3	(2)	4.14	[0.0114]	[2.5]	
	3	Cys	Zn–S	(1)	2.25	0.0003	2.5	0.043
		Imid + N/O	Zn–N/O	(4)	1.98	0.0045	2.2	
		Imidazole	Zn–C_5	(1)	2.93	0.0034	[2.2]	
		Imidazole	Zn–C_2	(1)	3.02	[0.0035]	[2.2]	
		Imidazole	Zn–C_4	(1)	4.08	[0.0048]	[2.2]	
		Imidazole	Zn–N_3	(1)	4.14	[0.0048]	[2.2]	
	4	Cys	Zn–S	(2)	2.22	0.0005	−1.8	0.048
		Imid + N/O	Zn–N/O	(3)	1.97	0.0054	−0.2	
		Imidazole	Zn–C_5	(1)	2.93	0.0084	[−0.2]	
		Imidazole	Zn–C_2	(1)	3.02	[0.0087]	[−0.2]	
		Imidazole	Zn–C_4	(1)	4.08	[0.0117]	[−0.2]	
		Imidazole	Zn–N_3	(1)	4.13	[0.0119]	[−0.2]	

tested in fit 1 is physically improbable. The two-sulphur single-imidazole-containing co-ordination sphere modelled in fit 4 $\{Zn(imid)_1(N,O)_2S_2\}$ is also an unlikely match to the 2° ADH Zn-liganding environment because of the unreasonably large Zn–S Debye–Waller α_{as}^2 values. Although either fit 2 or 3 in Table 2 is reasonable, if two imidazoles are assumed (fit 2) the Debye–Waller σ_{as}^2 values for outer shell scattering are 2–3-fold greater than those for the fit including a single imidazole (fit 3). Therefore, on the basis of this analysis, a 5- rather than a 4-co-ordinate Zn site of composition $Zn(N,O)_3(imid)_1S_1$ (fit 3, Table 2) is most consistent with the observed data (Figures 2b and 2c).

Mutant *adhB* genes encoding substitutions of residues 37, 59 and 150 were constructed by PCR to test the involvement of these amino acids in catalytic Zn binding. Mutant proteins were expressed at levels similar to, and purified to homogeneity using the procedure described for, the recombinant wild-type enzyme. Sequencing the mutated section of the *adhB* gene confirmed the identity of each mutant. Excess Zn was removed from the protein samples by extensive dialysis against buffer containing metal-chelating resin. Mutant and wild-type enzymes treated for Zn analysis were active and showed no increase in activity on addition of 10 μM Zn (results not shown); however, given the typically high affinities for enzyme catalytic metal binding, Zn-contaminated assay components could have provided sufficient metal to reconstitute the mutant enzyme catalytic sites, explaining the observed activity. All Zn levels measured by ICP-AES were more than 100-fold higher than the background value. ICP-AES analysis indicated that the enzyme expressed from the wild-type gene (pADHBKA4-kan) and the single N-terminal Met mutant enzyme bound 0.47 and 0.50 Zn^{2+} ions per subunit respectively. The C37S and H59N mutant enzymes contained less than 25 % of the Zn retained by the wild-type enzyme. Altering Asp^{150} to Glu preserved the wild-type Zn level, whereas that in the D150N mutant was 70 % of wild-type. Changing the putative Asp^{150} ligand to Cys increased bound Zn 2-fold. Finally, the Gly^{198} to Asp mutation did not significantly alter 2° ADH Zn content.

Point mutations altering Cys^{37}, His^{59} and Asp^{150} significantly reduced enzyme V_{max}(app) (Table 3). The conservative Cys^{37} to Ser mutation replaced the putative Zn ligand residue with one less than 0.4 Å shorter. This mutant retained less than 1 % of the wild-type enzyme V_{max}(app) toward both ethanol and propan-2-ol. Replacing His^{59} with Asn eliminated the ionizable nitrogen atom and reduced the enzyme V_{max}(app) to less than 0.5 % of that of the wild-type. The D150C mutant, which presumably mirrored the Cys-His-Cys 1° ADH catalytic Zn-liganding motif, retained approx. 3 % of the wild-type enzyme activity, the highest specific activity among the catalytic Zn mutants. Replacing the Asp carboxy moiety with a thiol group preserved its strong negative ionic character but shortened the amino acid side chain

Table 3 Effect of site-specific amino acid substitutions on *T. ethanolicus* 2° ADH activity

Propan-2-ol and ethanol kinetic values were determined with $NADP^+$ cofactor except in the case of the G198D mutant which displayed higher V_{max}(app) values using NAD^+ as the cofactor. $NADP^+$ kinetic values were determined with propan-2-ol as the co-substrate in all cases. Catalytic efficiency was defined as V_{max}(app)/K_m(app).

	Propan-2-ol			Ethanol			$NADP^+$		
Enzyme	V_{max}(app) (units/mg)	K_m(app) (mM)	Catalytic efficiency (ml/min per mg)	V_{max}(app) (units/mg)	K_m(app) (mM)	Catalytic efficiency (ml/min per mg)	V_{max}(app) (units/mg)	K_m(app) (mM)	Catalytic efficiency (ml/min per mg)
Wild-type	68	1.1	6.2×10^{-2}	19	53	3.6×10^{-4}	72	0.016	4.5
C37S	0.48	6.9	7.0×10^{-5}	0.042*	1100*	3.8×10^{-8}	0.48	0.0097	4.9×10^{-2}
D150C	2.0	1.4	1.4×10^{-3}	0.68	110	6.2×10^{-6}	2.0	0.00094	2.1
D150E	0.20	32	6.2×10^{-6}	0.028	180	1.6×10^{-7}	0.19	0.011	1.7×10^{-2}
D150N	0.60	0.20	3.0×10^{-3}	0.044	230	1.9×10^{-7}	0.64	0.037	1.7×10^{-2}
H59N	0.26	6.6	3.9×10^{-5}	0.017	38	4.5×10^{-7}	0.26	0.0060	4.3×10^{-2}
G198D	25	1.3	1.9×10^{-2}	7.9	110	7.2×10^{-5}	18	3.6	5.0×10^{-3}

* Approximate values estimated from assays at 700 and 350 mM ethanol only.

Table 4 Effect of the Gly^{198} to Asp mutation on *T. ethanolicus* 2° ADH nicotinamide cofactor preference

Propan-2-ol was used as the co-substrate in all cases. Cofactor efficiency was defined as the ratio of the catalytic efficiencies (V_{max}(app)/K_m(app)) for each cofactor form.

	$NADP^+$		NAD^+		Cofactor efficiency ratio ($NADP^+$/NAD^+)
Enzyme	V_{max}(app) (units/mg)	K_m(app) (mM)	V_{max}(app) (units/mg)	K_m(app) (mM)	
Wild-type	72	0.016	4.4	2.3	2400
G198D	18	3.6	25	0.76	0.15

by approx. 0.6 Å. Mutating Asp^{150} to Glu also retained the electronic characteristics for metal binding but it lengthened the side chain approx. 1.3 Å. The V_{max}(app) of this mutant was 0.2 % of the wild-type specific activity. Significantly reducing the polarity of this residue while maintaining wild-type geometry, the D150N mutant retained less than 1 % of the wild-type V_{max}(app).

Cofactor and substrate specificity

On the basis of the hypothesis of a specific amino acid position responsible for NAD(H) versus NADP(H) cofactor specificity in Rossmann-fold-containing proteins [41], our 1° ADH—2° ADH peptide alignment [28] predicts that mutating Gly^{198} in the *T. ethanolicus* 2° ADH peptide to Asp would exclude NADP(H) from the cofactor-binding site but allow NAD(H) binding. The wild-type enzyme had a 140-fold lower K_m(app) for $NADP^+$ than for NAD^+ and a catalytic efficiency for propan-2-ol oxidation 2400-fold greater using $NADP^+$ than using NAD^+ (Table 4). Replacing Gly^{198} with Asp increased the K_m(app) for $NADP^+$ 225-fold and reduced the V_{max}(app) using $NADP^+$ 4-fold. The mutant enzyme had a 3-fold lower K_m(app) toward NAD^+ and a 5.5-fold higher propan-2-ol-oxidation rate using NAD^+ compared with wild-type, giving the mutant a 6.7-fold lower catalytic efficiency for $NADP^+$-linked propan-2-ol oxidation than for the NAD^+-dependent reaction. In contrast with the G198D mutant, all of the enzymes containing mutations to the putative catalytic Zn-ligand residues had high affinities for $NADP^+$ [K_m(app) values less than 40 μM (Table 3)]. The high K_m(app) and low V_{max}(app) values using NAD^+ measured for these mutants were similar to those for the wild-type 2° ADH (results not shown).

Mutational effects on 2° ADH affinity for 1° compared with 2° alcohol substrates and on the catalytic efficiencies for oxidizing these substrates indicate a role for the putative catalytic Zn ligands in substrate specificity and in catalytic rate enhancement. Mutating Cys^{37} to Ser increased the K_m(app) values for propan-2-ol and ethanol 6-fold and 20-fold respectively (Table 3). Determining the K_m(app) for ethanol of the C37S mutant was complicated by our inability to measure enzyme initial rates using substrate concentrations greater than 700 mM and lower than 300 mM. This K_m(app) value is reported for completeness, but it is an approximate value and is not included in subsequent data analysis. Replacing His^{59} with Asn caused a 6-fold increase in the K_m(app) toward propan-2-ol and no significant change in the K_m(app) toward ethanol. The K_m(app) for propan-2-ol of the D150C mutant was similar to the wild-type value and that for ethanol was increased only 2-fold. Mutating Asp^{150} to Glu caused a 3-fold increase in the K_m(app) for ethanol but a 29-fold increase in the K_m(app) toward propan-2-ol. Finally, the D150N mutant had a K_m(app) toward propan-2-ol 5-fold lower than the wild-type and a K_m(app) toward ethanol 4-fold greater than the wild-type enzyme. The catalytic efficiencies of all mutants were lower than those of the wild-type enzyme but, for each mutant enzyme, the ratio of the catalytic efficiencies for propan-2-ol versus with ethanol oxidation varied from 4-fold lower (the D150E mutant) to 10-fold higher (the D150N mutant) than that calculated for the wild-type enzyme.

DISCUSSION

The research described here provides direct evidence for the involvement of specific amino acid residues in *T. ethanolicus* 39E 2° ADH catalysis. The presence of a single specifically bound Zn^{2+} ion in the enzyme subunit and the identities of at least two of the three potential liganding protein residues were confirmed by EXAFS analysis. ICP-AES data for the wild-type and mutant enzymes implicated Cys^{37}, His^{59} and Asp^{150} in catalytic Zn binding. Kinetic measurements of mutant enzymes implicated Cys^{37}, His^{59} and Asp^{150} in both catalytic rate enhancement and substrate specificity. Transforming the highly NADP(H)-specific *T. ethanolicus* 2° ADH into an NAD(H)-preferring enzyme with

the Gly[198] to Asp mutation further validated the sequence comparisons between 1° and 2° ADH, provided experimental evidence that this 2° ADH binds its nicotinamide cofactor in a Rossmann fold, and made the *T. ethanolicus* enzyme more suitable as an industrial biocatalyst. Furthermore construction of the overexpression system provided sufficient yield of purified enzyme for structural analysis and potential industrial-scale biocatalyst production.

The original *T. ethanolicus* 39E 2° ADH gene was expressed in *E. coli* DH5α under the control of its own promoter at approx. 2% of total protein [28]. In *E. coli* this construct generated a mixed 2° ADH population containing single and double N-terminal methionines, unlike the homogeneous single N-terminal methionine-containing population isolated from *T. ethanolicus*. Removing the native promoter region, placing the *adhB* gene under the control of the pBLuescriptII KS(+) lacZ promoter (in the pADHBKA4-kan construct), increased the 2° ADH expression to more than 10% of total protein. High-level expression of a homogeneous 2° ADH population containing a native-enzyme-like single N-terminal methionine was then achieved by modifying the pADHBKA4-kan *adhB* translational initiation ATGATG region to TTAATG (pADHB1M1-kan). A simplified purification procedure using only heat-treatment and $(NH_4)_2SO_4$ precipitation reduced enzyme losses to 33% while eliminating time-consuming and costly chromatography steps. The similar kinetic results reported here for the homogeneous and mixed recombinant enzyme populations and those reported previously for enzyme isolated from *T. ethanolicus* and the mixed recombinant protein [28] indicate that neither the additional Met residue nor its codon is needed for expression or processing of recombinant enzyme to a catalytically native-like 2° ADH. Expressing high levels of this homogeneous 2° ADH population and its isolation to extreme purity has allowed crystallographic studies for three-dimensional structural determination [19]. Economical recombinant 2° ADH production will also make the development of this enzyme as a commercial biocatalyst for chiral compound synthesis and racemate resolution [1–6,23] more feasible.

The prediction that Gly[198] was in part responsible for *T. ethanolicus* 2° ADH NADP(H) specificity was based on the hypothesis that the cofactor was bound in a Rossmann fold [28]. Consistent with the prediction from the hypothesis of Wierenga and Hol [41] that replacing Gly[198] with a negatively charged Asp residue would repel the added $NADP^+$ phosphate moiety, this mutation dramatically decreased the affinity of 2° ADH for $NADP^+$. However, mutating Gly[198] to Asp only increased the enzyme affinity for NAD^+ 3-fold which is still a 48-fold lower affinity than the wild-type enzyme for $NADP^+$. The mutant showed a 16000-fold increase in the ratio of the catalytic efficiencies for NAD^+ *versus* $NADP^+$ reduction but the V_{max}(app) of the mutant using either NAD^+ or $NADP^+$ was lower than that of the wild-type enzyme for $NADP^+$-dependent catalysis, suggesting that the G198D mutant–cofactor complex is suboptimal for turnover. Therefore, beyond agreement with the general prediction, the high mutant 2° ADH NAD(H) K_m(app) and low V_{max}(app) values indicate that other enzyme structural features contribute to NAD(H) *versus* NADP(H) binding and discrimination. This first experimental evidence that 2° ADHs bind cofactor in a Rossmann fold also generated the first thermophilic 2° ADH having higher catalytic efficiency using the more thermally stable NAD(H) cofactor.

With few exceptions, 1° ADHs require an enzyme-bound catalytic Zn^{2+} ion, liganded by two Cys residues and a single His residue [7]. The EXAFS data presented here identified a Zn^{2+} ion specifically bound to a co-ordination sphere $\{ZnS_1(imid)_1(N,O)_3\}$ including oxygen ligands plus a *T. ethanolicus* 2° ADH cysteine sulphur and imidazole nitrogen. This is similar to the co-ordination sphere reported for the 1° ADH catalytic Zn but inconsistent with the four cysteine sulphurs that co-ordinate the 1° ADH structural Zn [7]. The low ICP-AES measured Zn content ($\leqslant 1$ per subunit) also supports the predicted lack of a 1° ADH-like polycysteine-liganded structural Zn in 2° ADHs [27,28]. These EXAFS and ICP-AES analyses of the wild-type recombinant enzyme identifying a specifically bound Zn provide direct experimental evidence supporting the sequence- and chemical inactivation-based prediction that the *T. ethanolicus* 2° ADH contains a catalytic Zn [28]. However, kinetic analyses of site-directed 2° ADH mutants are required to identify the amino acid ligands and to confirm the catalytic importance of this bound metal.

Peptide alignments of 1° and 2° ADHs identified *T. ethanolicus* 2° ADH residues Cys[37] and His[59] as being analogous to two of the liver 1° ADH catalytic Zn ligands [24]. These alignments placed Asp[150] (conserved in 2° ADHs) in the sequence position corresponding to the second catalytic Zn–Cys ligand of liver 1° ADH. The nearest 2° ADH Cys residue to this position is Cys[203], C-terminal to the Rossmann-fold residue Gly[198]. Although a Cys-His-Asp Zn-binding motif has not been reported for ADHs, it has been described for sorbitol dehydrogenases [42]. Mutating Cys[37] to Ser, His[59] to Asn or Asp[150] to Asn eliminated them as potential Zn ligands and reduced enzyme activity to less than 1% of wild-type, implicating them in catalysis. The molar ratios of bound Zn per subunit for these mutants were 4-fold, 4-fold and 1.4-fold lower respectively than that for the wild-type enzyme, implicating them in Zn binding. The lack of a substantial change in bound metal as a result of the Gly to Asp mutation at position 198 (predicted to be unrelated to catalytic Zn liganding by sequence alignment and its demonstrated effect on cofactor specificity) further underscores the significance of the reduced Zn content measured for these position-37, -59 and -150 mutants. Altering Asp[150] to Glu indicated that maintaining the electronic nature of the Asp side chain preserved Zn binding, but the mutant's dramatically reduced V_{max}(app) (0.2% of wild-type) suggested that the position of the carboxylate was critical to catalysis. The D150C mutant, designed to create the 1° ADH-like Cys-His-Cys catalytic Zn-binding motif, doubled the molar ratio of enzyme-liganded Zn, implicating this residue in Zn binding by enhancing rather than diminishing metal content. The K_m(app) values resulting from this spatially conservative mutation were also less than those for the D150E mutant, suggesting that the metal position is important to enzyme affinity for substrate. Whether ICP-AES measured 2° ADH Zn-binding stoichiometry (one Zn per dimer) or gauged the enzyme's Zn affinity relative to that of the Chelex resin under the dialysis conditions does not alter the conclusion that 2° ADH affinity for Zn is specifically affected by non-conservative mutations at positions 37, 59 and 150. The ICP-AES measurements indicating that 10–100% of the five position-37, -59 and -150 mutant protein subunits bound metal after dialysis and the altered enzyme affinities for substrates also suggest that the low specific activities displayed by these mutants ($< 3\%$ of wild-type V_{max}(app) using either substrate) did not result simply from the loss of metal. Although analysis of this Zn-binding motif by EXAFS measurements of the mutant proteins or crystallographic determination of the 2° ADH three-dimensional structure is necessary to elucidate the enzyme–metal stoichiometry and the liganding structural details (both of these studies are underway), the EXAFS, ICP-AES and kinetic data reported here clearly support the hypothesis that *T. ethanolicus* 2° ADH residues Cys[37], His[59] and Asp[150] ligate a catalytic Zn.

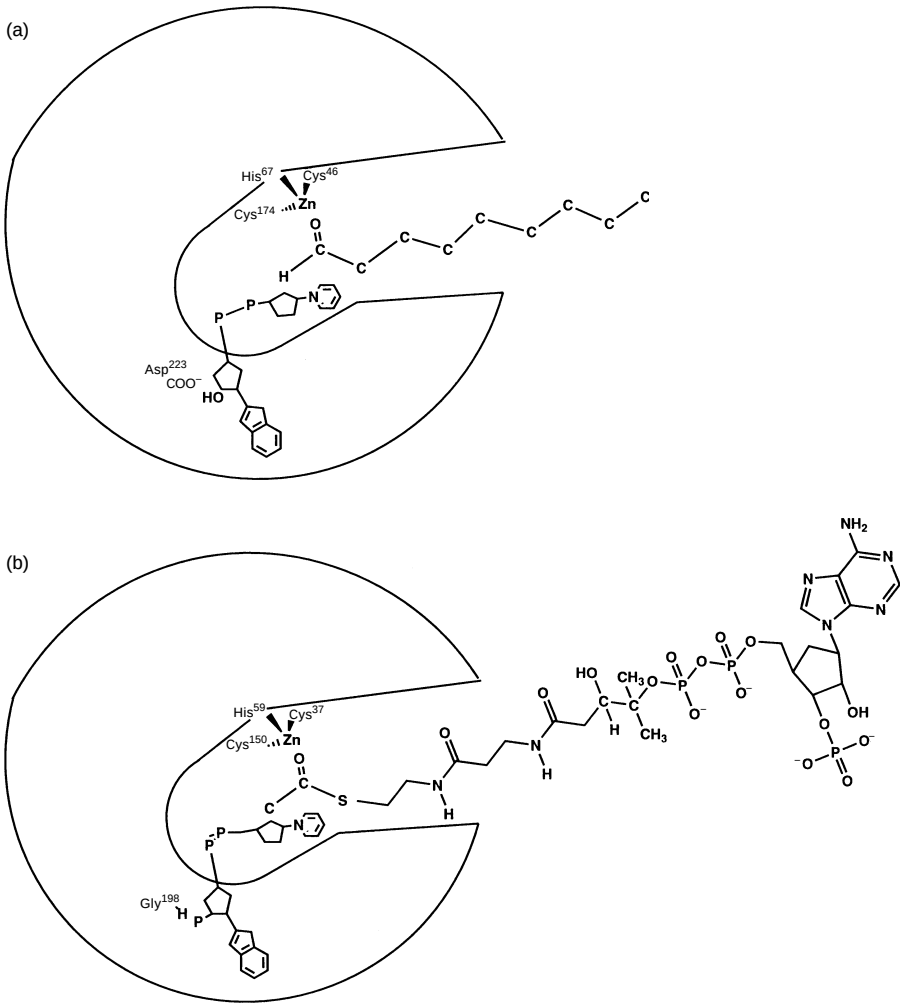

Figure 3 Comparison of 1° and 2° ADH active-site models

(**a**) The liver 1° ADH active site, and (**b**) the hypothesized 2° ADH active-site model incorporating the mutagenic and biophysical information.

Because horse liver 1° ADH is so well characterized, it is an excellent reference for predicting other ADH structures. 1° and 2° ADH peptide sequence comparisons have suggested that, although similarities exist, these enzyme groups may lack extensive structural similarity in catalytically important regions [27,28]. The data presented here demonstrate that the *T. ethanolicus* 2° ADH is a Zn-dependent Rossmann-fold-containing enzyme that uses a Cys-His-Asp metal-binding motif. Thus, by comparison with the liver 1° ADH (Figure 3a), we propose the hypothetical working model for 2° ADH structure–function studies depicted in Figure 3(b). The kinetic mechanisms proposed for catalysis by both horse liver [7] and *T. brockii* [43] ADHs require bound cofactor before substrate binding. Analysis of the horse liver 1° ADH three-dimensional structure [24] suggests that the cofactor may function to complete the active-site cavity wall. Therefore, as in the liver 1° ADH active site, the nicotinamide cofactor may complete 2° ADH catalytic pocket formation. The His^{59} and Asp^{150} mutations altered the 2° ADH K_m(app) for propan-2-ol over a 140-fold range, whereas the overall change in affinity for ethanol spanned a range of only 7-fold. The greater sensitivity of 2° ADH secondary-alcohol binding to Zn ligand mutations suggests that the substrate binds the catalytic Zn atom, as in the liver 1° ADH [7]. The physiological acetyl-CoA-linked reductive thioesterase activity for the *T. ethanolicus* 2° ADH also suggested that the long lobe of the previously proposed two-lobe active site [1] may be open-ended, allowing the CoA portion of the substrate to remain outside [17]. Analogously, the active-site channel in horse liver ADH has a closed short segment and a long segment open at the far end, with the catalytic Zn atom at their junction [24]. This may represent a structural similarity between 1° and 2° ADH architectures related to substrate specificity that is also of potential biotechnological importance. Finally, the data presented here indicate that comparative analysis between the two enzyme classes may yield further insights into both 1° and 2° ADH molecular structure–function relationships and obtaining an exact 2° ADH structure will provide the additional information needed to rigorously evaluate these hypotheses.

We gratefully acknowledge Maris Laivenieks for assistance in protein purification. Drs. Claire Vieille, Cindy Petersen and Lloyd Hough provided helpful discussions and assistance with 2° ADH molecular biology. X-ray absorption studies in the RAS laboratory are supported by the National Institute of Health (GM42025). The XAS data were collected at the Stanford Synchrotron Radiation Laboratory (SSRL), which is operated by the Department of Energy, Division of Chemical Sciences. The SSRL

Biotechnology Program is supported by the National Institute of Health, Biomedical Resource Technology Program, Division of Research Resources. Support for the X-ray fluorescence detector comes from the NIH BRS Shared Instrument Grant RR05648. This research was also supported by a grant from the Cooperative State Research Service, U.S. Department of Agriculture, under agreement 90-34189-5014.

REFERENCES

1 Keinan, E., Hafeli, E. K., Seth, K. K. and Lamed, R. L. (1986) J. Am. Chem. Soc. **108**, 162–169
2 Keinan, E., Hafeli, E. K., Seth, K. K. and Lamed, R. L. (1986) Ann. N. Y. Acad. Sci. **501**, 130–149
3 Hummel, W. (1990) Appl. Microbiol. Biotech. **34**, 15–19
4 Keinan, E., Seth, K. K., Lamed, R. L., Ghirlando, R. and Singh, S. P. (1990) Biocatalysis **4**, 1–15
5 Bradshaw, C. W., Fu, H., Shen, G.-J. and Wong, C.-H. (1992) J. Org. Chem. **57**, 1526–1532
6 Bradshaw, C. W., Hummel, W. and Wong, C.-H. (1992) J. Org. Chem. **57**, 1533–1536
7 Brändén, C.-I., Jörnvall, H., Eklund, H. and Furugren, B. (1975) Enzymes 3rd Ed., **11**, 103–190
8 Scopes, R. K. (1983) FEBS Lett. **156**, 303–306
9 Bleicher, K. and Winter, J. (1991) Eur. J. Biochem. **200**, 43–51
10 Dunn, M. F. and Hutchison, J. S. (1973) Biochemistry **12**, 4882–4892
11 Jacobs, J. W., McFarland, J. T., Wainer, I., Jeanmaier, D., Ham, C., Hamm, K., Wnuk, M. and Lam, M. (1974) Biochemistry **13**, 60–64
12 McFarland, J. T., Chu, Y.-H. and Jacobs, J. W. (1974) Biochemistry **13**, 65–69
13 Lamed, R. J. and Zeikus, J. G. (1981) Biochem. J. **195**, 183–190
14 Steinbüchel, A. and Schlegel, H. G. (1984) Eur. J. Biochem. **141**, 555–564
15 Bryant, F. O., Wiegel, J. and Ljungdahl, L. (1988) Appl. Environ. Microbiol. **54**, 460–465
16 Ismaiel, A. A., Zhu, C.-X., Colby, G. D. and Chen, J.-S. (1993) J. Bacteriol. **175**, 5097–5105
17 Burdette, D. S. and Zeikus, J. G. (1994) Biochem. J. **302**, 163–170
18 Zhang, Z., Djebli, A., Shoham, M., Frolow, F., Peretz, M. and Burstein, Y. (1993) J. Mol. Biol. **230**, 353–355
19 Arni, R. K., Watanabe, L., Fontes, M., Burdette, D. S. and Zeikus, J. G. (1996) Protein Pept. Lett. **3**, 423–426
20 Korkhin, Y., Frolow, F., Bogin, O., Peretz, M., Kalb, A. J. and Burstein, Y. (1996) Acta Crystallogr. **D52**, 882–886
21 Lovitt, R. W., Longin, R. and Zeikus, J. G. (1984) Appl. Environ. Microbiol. **48**, 171–177
22 Lamed, R. J., Keinan, E. and Zeikus, J. G. (1981) Enzyme Microbiol. Technol. **3**, 144–148
23 Zheng, C., Pham, V. T. and Phillips, R. S. (1992) Bioorg. Med. Chem. **2**, 619–622
24 Eklund, H., Nordström, B., Zeppezauer, E., Söderlund, G., Ohlsson, I., Boiwe, T. and Brändén, C.-I. (1974) FEBS Lett. **44**, 200–204
25 Rossmann, M. G. and Argos, P. (1976) J. Mol. Biol. **105**, 75–95
26 Jendrossek, D., Steinbuechel, A. and Schlegel, H. G. (1988) J. Bacteriol. **170**, 5248–5256
27 Peretz, M. and Burstein, Y. (1989) Biochemistry **28**, 6549–6555
28 Burdette, D. S., Vieille, C. and Zeikus, J. G. (1996) Biochem. J. **316**, 115–122
29 Nagata, N., Maeda, K. and Scopes, R. K. (1992) Bioseparation **2**, 353–362
30 Oka, A., Sugisaki, H. and Takanami, M. (1981) J. Mol. Biol. **147**, 217–226
31 Sambrook, J., Fritsch, E. F. and Maniatis, T. (1989) Molecular Cloning: A Laboratory Manual, 2nd edn., (Nolan, C., ed.), Cold Spring Harbor Laboratory Press, Cold Spring Harbor, NY
32 Ausubel, F. M., Brent, R., Kingston, R. E., Moore, D. D., Seidman, J. G., Smith, J. A. and Struhl, K., eds., (1993) Current Protocols in Molecular Biology, Greene Publishing and Wiley-Interscience, New York
33 Sanger, F., Nicklen, S. and Coulson, A. R. (1977) Proc. Natl. Acad. Sci. U.S.A. **74**, 5463–5467
34 Brooks, S. (1992) Biotechniques **13**, 906–911
35 Scott, R. A. (1985) Methods Enzymol. **117**, 414–458
36 Bear, C. A., Duggan, K. A. and Freeman, H. C. (1975) Acta Crystallogr. Sect. B **31**, 2713
37 Rehr, J. J. and Albers, R. C. (1990) Phys. Rev. B **41**, 8139–8149
38 Mustre de Leon, J., Rehr, J. J., Zabinski, S. I. and Albers, R. C. (1991) Phys. Rev. B **44**, 4146–4156
39 Rehr, J. J., Mustre de Leon, J., Zabinski, S. I. and Albers, R. C. (1991) J. Am Chem. Soc. **113**, 5136–5140
40 Coucouvanis, D., Patil, P. R., Kanatzidis, M. G., Delering, B. and Baenziger, N. C. (1985) Inorg. Chem. **24**, 24–31
41 Wierenga, R. K. and Hol, G. J. (1983) Nature (London) **302**, 842–844
42 Karlsson, C., Jornvall, H. and Hoog, J. O. (1995) Adv. Exp. Med. Biol. **372**, 397–406
43 Pereira, D. A., Gerson, F. P. and Oestreicher, E. G. (1994) J. Biotechnol. **34**, 43–50

Received 13 January 1997/22 April 1997; accepted 7 May 1997